5-9-2011

Codoping in a single molecular junction from first principles

Subhasish Mandal
Michigan Technological University

Ranjit Pati
Michigan Technological University

Codoping in a single molecular junction from first principles

Subhasish Mandal and Ranjit Pati
Department of Physics, Michigan Technological University, Houghton, Michigan 49931, USA
(Received 19 October 2010; revised manuscript received 16 January 2011; published 9 May 2011)

Using a codoping model, where a cation and an anion are introduced simultaneously into the host to maintain charge neutrality, we probed the electron transport characteristics in a single molecular junction. We used the 1, 12-dicarba-*closo*-dodecaborane inorganic molecule as a precursor, replaced one of the vertex carbon atoms by a boron atom, and simultaneously decorated it with an endohedrally doped alkali atom (Li or Na) to look into the role of dopant atoms in the conductivity. The commonly used thiolate anchoring groups are used to attach the molecule between two gold electrodes, and a parameter-free, first-principles, single-particle Green's function approach is used to calculate the current-voltage characteristics. When compared to the undoped system, a significant increase in current is observed for the system codoped with Na and B; about an order of magnitude increase in the observed current is found at an applied bias of ∼2 V. Charge transfer from the alkali atom to the host is found to have a profound effect on the electronic structure, causing a dramatic change in the conductivity. Since the single alkali atom controls the behavior of electron flow in this circuit, we call this device a "single-atom-controlled" device.

DOI: 10.1103/PhysRevB.83.195420 PACS number(s): 73.63.−b, 85.65.+h, 73.50.Fq, 71.10.−w

I. INTRODUCTION

Doping, a scheme for tuning electronic, magnetic, and optical properties of materials by purposely introducing a small amount of impurities, has played a fundamental role in the rapid advancement of silicon-based semiconductor technologies since its inception. With the size of silicon-based semiconductor devices approaching their fundamental limit of miniaturization, researchers are relentlessly looking for alternative quantum-controlled materials and schemes at the nanometer to subnanometer dimension to overcome the impasse blocking the realization of smaller, faster, and more powerful electronic devices.[1] Several groups have already started looking at the doping scheme via exploring the role of dopants in modulating the electronic structure of nanocrystals and molecular nanostructures.[2–7] The strong quantum confinement effect makes these nanomaterials highly sensitive to dopant atoms; even a single dopant atom has been found to have a profound impact on the electronic structure, causing dramatic changes in the electrical properties of these materials. A well-known example is the superconductive characteristic found in alkali-doped C_{60}.[8–11] It has been revealed that a dopant atom changes the electronic structure by donating or accepting charge to or from the host system.[12]

However the "conventional controlled doping of a single atom"[13] has been found to be exceedingly difficult when the size of the host system is reduced to the molecular length scale. To overcome such difficulties, progress has been made through the discovery of a variety of synthetic approaches,[14] resulting in the synthesis of a range of new molecular compounds.[15] One example is the synthesis of polyhedral *closo*-boranes and *closo*-carborane structures.[16–19] These important classes of boron-rich structures have been explored as boron carriers in boron-neutron-capture therapy and as molecular probes in medical diagnostics.[20–22] Researchers have also studied electron transfer properties of 10-, and 12-vertex carborane structures for their possible application in electronics.[23] Despite their rich chemistry, these inorganic cage structures have never been considered large enough to encapsulate a dopant atom. It was first shown by Jemmis and coworkers[24] that *closo*-boranes can be doped endohedrally to enhance their stability. Subsequently, Oliva and colleagues have used high-level quantum chemistry calculations to demonstrate that the lithium-encapsulated carborane structure ($Li@C_1B_{11}H_{12}$)[25] can be used as an effective-mass-selective conveyor via photochemical switching.[26] These pioneering works suggest that a rich fundamental science remains to be explored for such small inorganic cage structures. For example: How would doping a single atom affect the electronic structure of such a small inorganic host? Can a single atom play a vital role in controlling the flow of electrons in a molecular junction?

To answer some of these subtle questions, we have considered the precursor 1, 12-dicarba-*closo*-dodecaborane complex and used a codoping model by replacing one of the vertex carbon atoms by a boron atom and decorating it with an endohedrally doped, electron rich, alkali atom ($X@C_1B_{11}H_{12}$, $X =$ Li or Na) to investigate the role of the dopant on its electronic structure. Subsequently, prototype two-terminal device structures are built from each of these individual molecules by sandwiching them between two gold electrodes, and a parameter-free, first-principles, single-particle Green's function approach is used to study their current-voltage characteristics. The commonly used thiolate (-S) anchoring groups are used to attach the molecule between the gold electrodes. The codoping approach allows us to maintain the charge neutrality of the molecule-electrode system. It should be noted that this type of codoping model, where a cation and an anion are simultaneously introduced into the host, has been adopted to tune the optical properties of TiO_2 semiconductors.[27] Our calculations reveal that the conductivity in an $X@C_1B_{11}H_{12}$ junction, where $X =$ Li or Na, is significantly higher than that in a $C_2B_{10}H_{12}$ junction. Further analysis shows that the dopant alkali atom donates electronic charges to the cage ($C_1B_{11}H_{12}$), resulting in a profound effect on its electronic structure, and therefore on its conductivity—opening up a path toward a single-atom-controlled device.

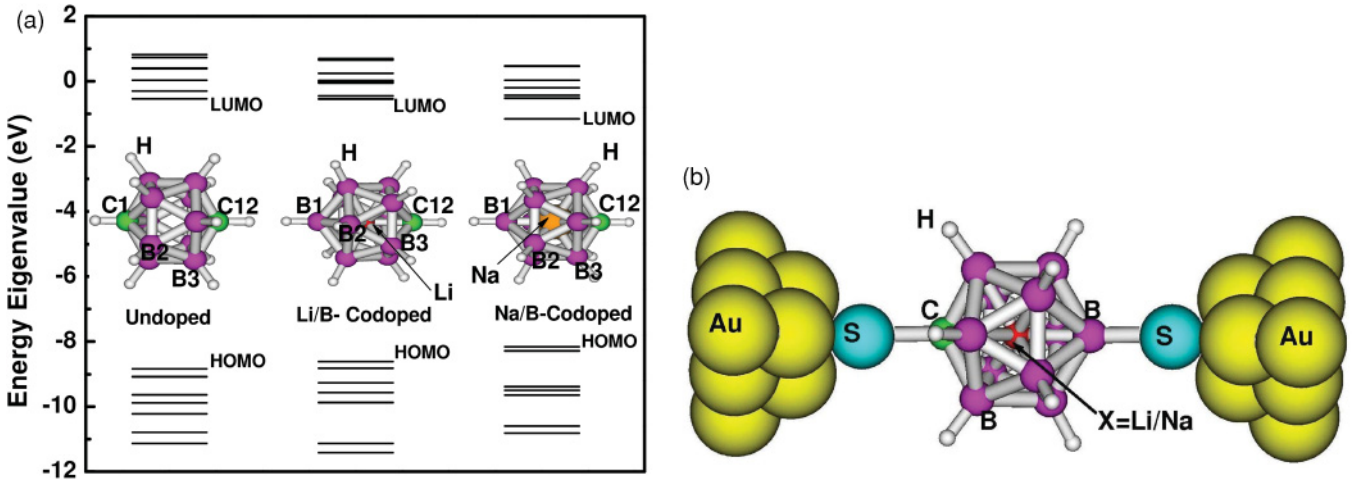

FIG. 1. (Color online) (a) Energy eigenvalues of $C_2B_{10}H_{12}$, $Li@C_1B_{11}H_{12}$, and $Na@C_1B_{11}H_{12}$. Respective optimized structures are shown in the inset. (b) Schematic representation of alkali (X = Li, Na) carborane junction codoped with B.

The rest of the paper is organized as follows. The computational approach adopted here is described briefly in Sec. II followed by results and discussions in Sec. III. Our main findings are summarized in Sec. IV.

II. COMPUTATIONAL APPROACH

We used the 1, 12-dicarba-*closo*-dodecaborane ($C_2B_{10}H_{12}$) molecule as a precursor (Fig. 1), and adopted a simple codoping model to introduce atomic impurities into the host. We replaced one of the vertex carbon atoms in $C_2B_{10}H_{12}$ by a boron atom and decorated it simultaneously with an endohedrally doped alkali atom ($X@C_1B_{11}H_{12}$, X = Li or Na) to maintain the charge neutrality [Fig. 1(a)]. The geometry optimizations are performed using density functional theory, which involves Becke's three-parameter hybrid functional (B3LYP)[28,29] for exchange and correlation. A real-space approach, in which the many-body single determinant wave function of the electron is expanded in terms of a finite set of Gaussian atomic orbitals,[29] is used for this calculation. We utilized a triple-valence zeta basis set augmented by polarization and diffuse functions (6-311++G**) to carry out these calculations.

Next, a prototypical two-terminal molecular device is built from each of these molecular complexes by sandwiching them between two semi-infinite gold electrodes; thiolate (-S) anchoring groups are used to attach the molecule between the electrodes [Fig. 1(b)]. To model such an open device structure, we have divided it into two parts. The first part is the active scattering region, which consists of the molecular part of the device and a finite number of gold atoms from the Au (111) surface. Particularly, we embedded the molecule with thiolate (-S) anchoring groups between two clusters of three Au atoms, each taken from the Au(111) surface; S is incorporated into the three-fold hollow site of the Au atoms.[30,31] These Au-atoms are assumed to be perturbed when the molecule adsorbs onto the electrode surface. In principle, the inclusion of a large number of Au atoms would better reflect the effect of the electrodes. However, it is a big computational challenge to carry out the electronic structure calculation by incorporating a large number of Au atoms in the active region, where each atom is expanded in terms of Gaussian atomic orbitals. For practical purposes, we have used only three Au atoms on each side of the molecular wire to which the S atom is directly bonded. The single electron energy levels in this finite region in the presence and absence of bias is calculated using the same real-space, finite-cluster density functional approach as used for the free molecule. For the gold atoms, the Los Alamos double zeta effective-core-potential basis set[29] that includes the scalar relativistic effects is used. During the self-consistent calculation and to ensure tight convergence, the convergence criterion for energy, maximum, and root-mean-square electron density are set at 10^{-6}, 10^{-6}, and 10^{-8} atomic units, respectively. The Hamiltonian in the presence of applied bias for the active scattering region is calculated as follows:[32]

$$H(\epsilon) = H(0) + \vec{\epsilon} \cdot \sum_i \vec{r}(i), \tag{1}$$

where $H(0)$ is the Hamiltonian in the absence of the electric field, $\vec{\epsilon}$ is the applied dipole electric field, and $\vec{r}(i)$ is the coordinate of the ith electron. It should be noted that the ground-state-based density-functional-theory (DFT) approach, which is used here to evaluate $H(\epsilon)$, has limitations in predicting the excitation energy. An accurate description of the excitation requires approaches beyond mean-field theory,[33] such as configuration interaction,[34,35] coupled cluster,[36] or the many-body GW approach.[37] Although some of these higher-level methods have been explored in the context of transport in molecular junctions, their complete implementation is prohibitively difficult both in the time-independent or time-dependent framework; the time-dependent formalism would be more appropriate.[38–44] It is important to note that transport in molecular junctions not only requires the accurate energy level description of the molecular spacer but also depends on the precise determination of the coupling between the molecule and the semi-infinite electrode. In particular, for the latter case, the higher-level approaches are difficult to implement. In addition, the requirement to include the bias effect self-consistently compounds the difficulty. The

ground-state-based DFT approach[41,45–53] has been quite successful in explaining the experimental results qualitatively and, in some instances, quantitatively. Here, we have considered a strongly coupled chemically bonded junction, where the coupling between molecule and lead plays a more dominant role. In such a scenario, the ground-state-based DFT approach would be a reasonably good approximation to treat electronic current.

The second part of the prototype device that represents the rest of the electrode is essentially unperturbed by the molecular adsorption and is assumed to retain its bulk properties. We have used the plane-wave-based periodic DFT to model this portion of the device. Subsequently, we use the single-particle Green's function approach to couple the finite and the bulk part of the model device. A brief description of this approach is described below. In this mean-field approach, the single-particle Green's function,[30,45,46,50,51,54] which has an implicit bias dependence, is calculated as follows:

$$G(E,\epsilon) = [E \times S - H_{\mathrm{MOL}}(\epsilon) - \Sigma_L(\epsilon) - \Sigma_R(\epsilon)]^{-1}. \quad (2)$$

$H_{\mathrm{MOL}}(\epsilon)$ is the orthogonalized bias-dependent Kohn-Sham molecular Hamiltonian obtained by suitable partitioning of $H(\epsilon)$. The use of the real-space approach for the active scattering region allows us to partition the $H(\epsilon)$ to obtain $H_{\mathrm{MOL}}(\epsilon)$. E is the injection energy of the tunneling electron, and S is an identity matrix. $\Sigma_{L,R}(\epsilon)$ are the bias-dependent self-energy functions, which depict the interaction between the molecule and the lead. They are calculated as follows:

$$\Sigma_{L,R}(\epsilon) = C^{\dagger}_{L,R} G_P(E) C_{L,R}, \quad (3)$$

where $C_{L,R}$ are the orthogonalized bias-dependent molecule-lead coupling matrices. This approach allows us to explicitly include the nonequilibrium nature of the interfacial electronic coupling into our model. G_P, which is the Green's function of the lead, is calculated as follows:

$$G_P(E) = -i\pi\rho(E) I_P, \quad (4)$$

where I_P is an identity matrix of dimension $P \times P$ and P is the total number of Gaussian basis functions used to represent the Au atoms in the active scattering part of the device. $\rho(E)$, which is the normalized $s^1 d^{10}$ density of states (DOS) of the three-dimensional (3D) gold, is obtained by using the projector-augmented-wave (PAW) approach within the periodic DFT calculations as implemented in the VASP code.[55] We have used $51 \times 51 \times 51$ k-point sampling within the Monkhorst-Pack scheme to sample the Brillouin zone. For $\rho(E)$, the energy grid is taken as 0.001 eV; the same energy grid is used for the integration in Eq. (5) to calculate the current. We have aligned the Fermi energy level of the active region of the device at equilibrium with the Fermi energy of the bulk gold. The current as a function of applied bias is then calculated within coherent scattering approximation using the multichannel Landauer-Büttiker formalism.[30,52,53,56,57] The expression for the current is

$$I_{SD} = \frac{2e}{h} \int_{\mu_1}^{\mu_2} T(E,V)[f(E,\mu_2) - f(E,\mu_1)]dE, \quad (5)$$

where $T(E,V)$ is the bias-dependent transmission function[53,56] and is given by

$$T(E,V) = \mathrm{Tr}(\Gamma_L G \Gamma_R G^{\dagger}), \quad (6)$$

where $\Gamma_{L,R} = i(\Sigma_{L,R} - \Sigma^{\dagger}_{L,R})$.

In Eq. (5), e is the electronic charge, h is Planck's constant, and f is the Fermi distribution function. $\mu_{1,2}$ are calculated as follows:

$$\mu_{1,2} = E_f \mp V_{\mathrm{LOW,HIGH}}, \quad (7)$$

where E_f is the equilibrium Fermi energy. V_{LOW} and V_{HIGH} are calculated self-consistently[53] for each applied dipole field from the difference between the average electrostatic potentials[58] at finite and zero bias at the respective electrode. The average electrostatic potential at the respective electrode (left or right) is calculated by averaging the electrostatic potential of gold atoms over the number of gold atoms (left or right) in the active region of the device.

The potential difference V_{SD} is then calculated from the difference between V_{LOW} and V_{HIGH}; at equilibrium $V_{\mathrm{LOW}} = V_{\mathrm{HIGH}}$. We have also subtracted (added) a small thermal smearing term, $k_B T$ (=0.026) from (into) the lower (upper) limit of the integration in Eq. (5) to account for the electronic temperature at the interface in the nonequilibrium condition.

III. RESULTS AND DISCUSSIONS

A. Electronic structure of codoped and undoped molecules

The optimized structures and the energy eigenvalues of undoped and doped molecules are presented in Fig. 1(a). The structural details including the formation energy (Δ_{FE}) are summarized in Table. I. The formation energy is calculated as $\Delta_{\mathrm{FE}} = (E_{\mathrm{MOL}} - \Sigma E_I)/\Sigma_I$, where E_{MOL} is the total energy of the molecule; E_I is the energy of the atom present in the molecule, and Σ_I is the total number of atoms. It is clear from the values of Δ_{FE} (Table. I) that these three systems are stable. One can also notice from Table. I that

TABLE I. Calculated Δ_{FE} (eV/atom) and bond lengths in carborane molecules undoped, codoped with Li and B, and codoped with Na and B.

Molecule	Δ_{FE}(eV/atom)	Atoms[a]	Bond Length (Å)
$C_2B_{10}H_{12}$	−4.48	C(1)-C(12)	3.05
		C(1)-B(2)	1.71
		B(2)-B(3)	1.77
$Li@C_1B_{11}H_{12}$	−4.26	B(1)-C(12)	3.43
		C(12)-B(3)	1.79
		B(1)-B(2)	1.90
		B(2)-B(3)	1.86
		B(1)-Li	1.74
		C(12)-Li	1.69
$Na@C_1B_{11}H_{12}$	−3.55	B(1)-C(12)	3.73
		C(12)-B(3)	1.91
		B(1)-B(2)	2.12
		B(2)-B(3)	1.98
		B(1)-Na	1.88
		C(12)-Na	1.86

[a]Labeling of the atoms is shown in Fig. 1(a).

the bond lengths of *p*-carborane (p-$C_2B_{10}H_{12}$) compare very well with the previously reported theoretical and experimental values. The electron diffraction study reported the structure of *p*-carborane to be slightly distorted from the icosahedron symmetry with C(1)-B(2) and B(2)-B(3) bond lengths of 1.710 and 1.792 Å, respectively.[59] The theoretical calculation at the MP2 level reported the C(1)-B(2) and B(2)-B(3) bond lengths are 1.703 and 1.781 Å, respectively.[60] These data are in excellent agreement with our calculated values of 1.71 and 1.77 Å for the respective bond lengths.

We then calculated the energy for the positively charged state of the *p*-carborane and compared that with the energy of the neutral state to obtain the ionization potential (IP) value of 10.87 eV, which is in good agreement with the reported experimental IP of 10.6 eV.[61] For the doped molecules, the structural details are not available for comparison. From Table. I, the distance between the two vertex atoms in $C_2B_{10}H_{12}$ is found to be 3.05 Å, which increases to 3.43 Å in $Li@C_1B_{11}H_{12}$. In $Na@C_1B_{11}H_{12}$, the distance between the vertex atoms (C and B atoms) is found to be 3.73 Å. Similar expansion in C-B and B-B bond lengths upon codoping are noted in Table. I. The expansion of the cage structure upon codoping has important implications on their electronic structures, as revealed by the eigenvalue spectrum [Fig. 1(a)]. Upon codoping of Li at the endohedral site and B at the substitutional site, the highest occupied molecular orbital (HOMO) level in $Li@C_1B_{11}H_{12}$ shifted upward but the lowest unoccupied molecular orbital (LUMO) level remained almost at the same position, resulting in a reduction of the HOMO-LUMO gap (ΔE_g) from 8.29 eV to 8.07 eV. In $Na@C_1B_{11}H_{12}$, the HOMO level shifted upward and the LUMO level shifted downward, resulting in a further reduction of ΔE_g, which was found to be 7.01 eV.

To gain further insight, we carried out the Mulliken charge analysis for the undoped and doped molecules. In *p*-carborane, all the boron atoms are negatively charged and all the carbon atoms are positively charged. However in $Li@C_1B_{11}H_{12}$ and $Na@C_1B_{11}H_{12}$, the Li and Na have positive charges; negative charges are distributed on the rest of the B and C atoms. The strong polarization effect in $X@C_1B_{11}H_{12}$, where X = Li or Na, suggests that these alkali atoms have a strong influence on their electronic structure.

Now the following question arises: Will the observed strong influence of alkali atoms in the free molecule have a measurable effect on the conductivity of the device? To address this question, we built a prototype device [Fig. 1(b)] as discussed in Sec. II. Since the atomic level structural details at the molecule-lead interface are not available *a priori*, we varied the S-Au distance in the active part of the device to find the equilibrium configuration. In the *p*-carborane system, the optimized S-Au distance is found to be 2.77 Å. As our aim is to explicitly investigate the effect of dopant atoms on the conductivity, we have kept the interfacial contact structure the same for all systems.

B. Potential profile

To model the device in the nonequilibrium condition and to understand the electronic response of the molecule, we applied a dipole electric field along the molecular wire axis as discussed in Sec. II. We calculated the electrostatic potential (EP) self-consistently at each atomic center in the active part of the device in the presence and absence of applied field; in the nonequilibrium condition the EP is obtained as a function of external applied field. Subsequently, the difference of EP between the equilibrium ($V_{\mathrm{HIGH}} = V_{\mathrm{LOW}}$) and nonequilibrium situations ($V_{\mathrm{HIGH}} \neq V_{\mathrm{LOW}}$) is averaged over the degrees of freedom perpendicular to the wire axis to obtain the relative electrostatic potential (REP). The REP values at each atomic center are then plotted as a function of applied bias (V_{SD}) along the molecular wire axis (Fig. 2).

In Fig. 2(a), the potential profile for three systems at $V_{SD} \sim 1$ V is presented. First, from Fig. 2(a), a sudden drop in potential is noticed at the Au-S junctions for the undoped carborane system. Second, the two terminal S atoms for the $C_2B_{10}H_{10}$ system are located at the valley and hill of the potential profile, respectively, exhibiting a field-induced polarization effect. Third, there is an effective potential barrier between the two terminal S atoms. However, for the codoped system, at the left S-Au junction, a steady drop in potential is observed in contrast to an abrupt change in potential at the right S-Au junction. For the codoped system, the effective barrier height between the terminal S atoms is significantly smaller than that in the undoped system; this could have a significant effect on the conductivity. The observed asymmetric feature in potential drops at the Au-S junction in the codoped systems, which is due to the structural asymmetry at the vertex position; the opposite-vertex atoms in the codoped systems are C and B atoms.

In Figs. 2(b), 2(c), and 2(d), we summarize the potential profile for undoped, Li/B-codoped, and Na/B-codoped systems, respectively. For the undoped system at $V_{SD} = 1.99$ V, the magnitude of potential drop from Au to S on the left is found to be 0.69 V; on the right Au-S junction the potential drop is found to be 0.88 V. In the case of the $Li@C_1B_{11}H_{10}$ system, at 2.06 V, a smaller potential drop of 0.41 V is observed on the left Au-S junction in contrast to a larger drop of 0.60 V on the right. A similar steady drop of 0.46 V on the left junction and a larger drop of 0.71 V is found in the $Na@C_1B_{11}H_{10}$ system at 2.06 V. A closer examination reveals a significant change in the potential profile as a function of applied V_{SD}, suggesting that inclusion of the bias effect is essential to understand the electronic response of the molecular device.

C. Current-voltage characteristics

The calculated current-voltage characteristics for undoped, Li/B-codoped, and Na/B-codoped systems are summarized in Fig. 3(a). First, for the undoped system, a steady increase in current with increasing applied bias is noted. For the codoped systems, the calculated current is found to be significantly higher than the undoped system. For example, at 1.99 V, for the undoped system, the calculated I_{SD} is found to be 0.96 mA. For the system codoped with Li and B, the calculated I_{SD} is found to be 4.11 mA at 1.93 V, and, for the system doped with Na and B, the I_{SD} is found to be 8.07 mA at 1.86 V, which is ~8 times higher than that in the undoped system. The twofold increase in current from the $Li@C_1B_{11}H_{10}$ system to the $Na@C_1B_{11}H_{10}$ system suggests that the single alkali atom (Na or Li) plays a dominant role in controlling the conductivity of these molecular junctions; this could potentially lead to an

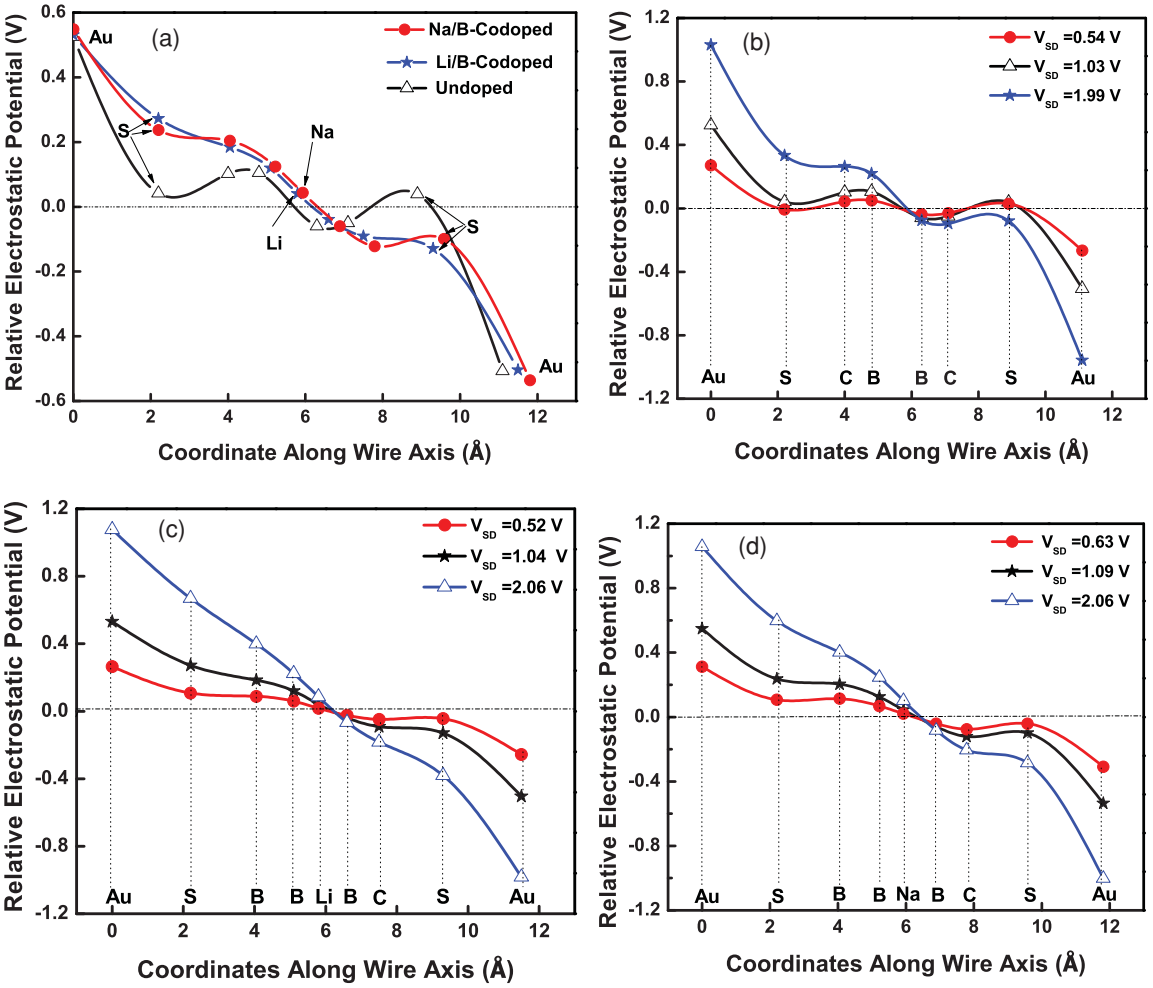

FIG. 2. (Color online) (a) Potential profile of undoped junctions and junctions codoped with Li and B and with Na and B at $V_{SD} \sim 1$ V. (b) Bias-dependent potential profile for undoped junctions, (c) junctions doped with Li and B, and (d) junctions doped with Na and B. The vertical dotted lines depict the location of the atoms along the wire axis in the device.

ultimate single-atom-controlled device. Further examination of Fig. 3(a) reveals a nonlinear feature in current above $V_{SD} \sim 1$ V in the system codoped with Na and B in contrast to a linear behavior in current for the undoped systems and the systems codoped with Li and B.

D. Bias-dependent transmission

To understand the significant increase in current upon codoping and to account for the observed nonlinear feature in current for the system codoped with Na and B, we calculated the bias-dependent transmission as a function of injection energy. The results are presented in Figs. 3(b) and 3(c). The chemical-potential window is shown by the dotted line (the Fermi energy is set to zero in the energy scale). For brevity, we considered only two bias points. It is important to note that, unlike the previous systems,[30,53] where we reported much smaller values for total transmission using the same approach, we found much higher values for $T(E,V)$ in the codoped systems. There are several reasons that can be given for such high transmission. First, the single-particle approach to obtain transmission (where the dynamical corrections are not included) overestimates the total transmission by at least an order of magnitude. This has been pointed out recently by several authors.[62,63] Second, a strong metal-induced screening, resulting in a significant broadening of the molecular energy level, is expected to yield a higher total transmission. Third, a strong charge polarization, introduced due to simultaneous doping of oppositely charged ions into the host, also plays a major role in increasing the magnitude of transmission. A higher value for total transmission in doped C_{60} has also been reported.[7]

Next, we turn to the relative trends for transmission between the undoped and codoped systems, which is the main focus of this work. In the system codoped with Na and B the transmission is considerably higher than that in the undoped system. For example, at $V_{SD} \sim 2$ V, the transmission for $Na@C_1B_{11}H_{10}$ at an injection energy of 1.0 eV is 116.85 as compared to 11.6 for the undoped system. This ten-fold increase in transmission for $Na@C_1B_{11}H_{10}$ compared with the undoped system accounts for the ~ 8 times increase in current at ~ 2 V for the former. In the system codoped with Li and B, $T(E = 1.0, V_{SD} \sim 2\text{ V})$ is found to be 42.04. At $V_{SD} \sim 1$ V, for an injection energy of 0.5 eV, $T(E,V)$ is found to be 5.9 for

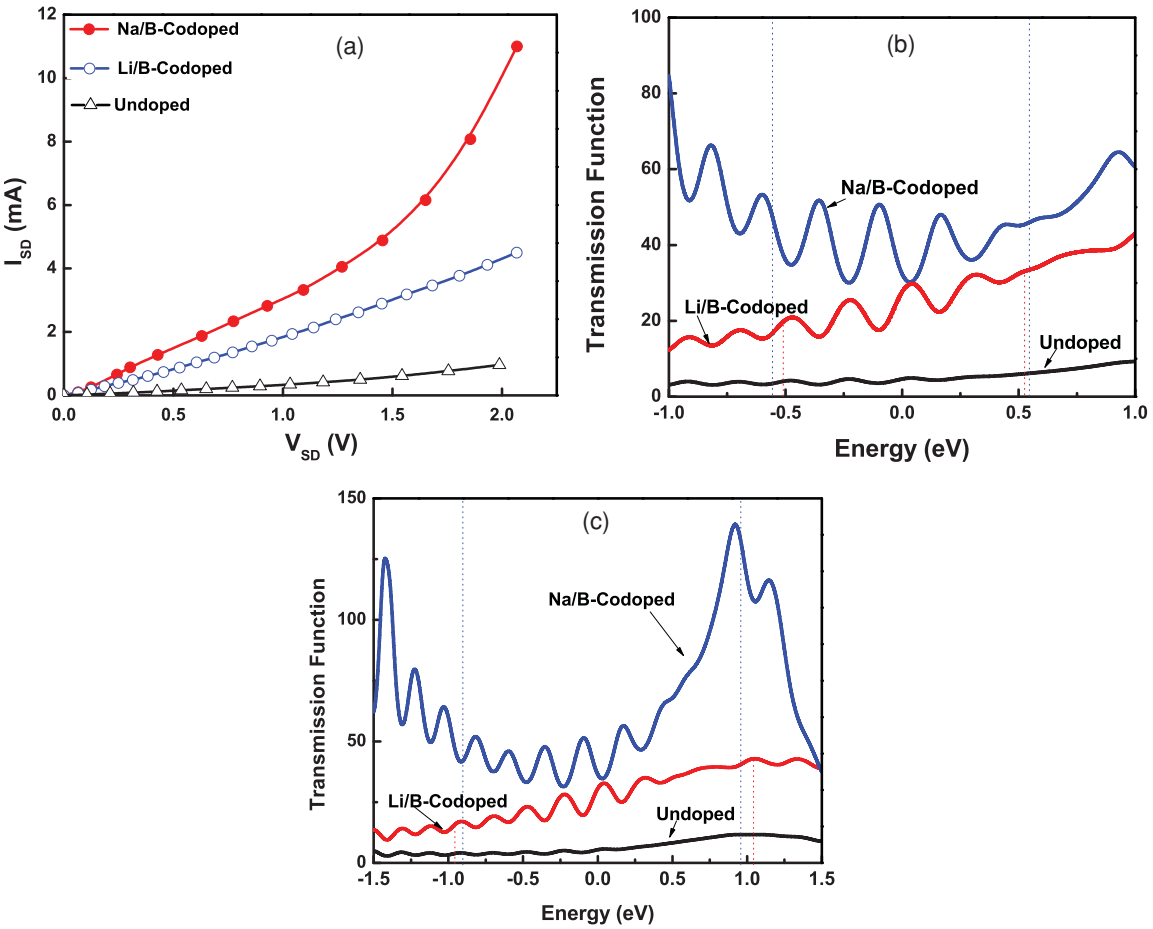

FIG. 3. (Color online) (a) Current-voltage characteristic of undoped junctions and junctions codoped with Li and B and with Na and B. (b) Bias-dependent transmission as a function of injection energy at (b) ∼1 V and (c) ∼2 V. The Fermi energy is set to zero in the energy scale and the dotted lines represent the chemical-potential window.

the undoped system compared to 45.13 for $Na@C_1B_{11}H_{10}$. By comparing $T(E,V)$ in Figs. 3(b) and 3(c), one can notice that there is a steep increase of $T(E,V)$ with increasing injection energy from 0 to 1 eV for the system codoped with Na and B at ∼2 V whereas, for the systems codoped with Li and B and the undoped systems, a steady increase is observed in $T(E,V)$ with increasing injection energy. Thus, the rapidly increasing area under $T(E,V)$ with increasing bias for the system codoped with Na and B is responsible for the observed nonlinear behavior of current above ∼1 V.

To identify the origin of the oscillations seen in $T(E,V)$, we replace the oscillating function $\rho(E)$ in Eq. (4) by a constant value of 0.03 (which is approximately equal to the s-band DOS of bulk gold at the Fermi energy) and recalculated $T(E,V)$; no oscillation was found. This clearly suggests that the observed oscillation in $T(E,V)$ is due to $\rho(E)$. However, it does not explain the observed strong oscillation in codoped systems. It should be noted that $\rho(E)$ has a small oscillating feature, which varies between 0.022 and 0.031 within the chemical-potential window [Fig. 3(b)]. The other possible reason for the observed oscillation could be the backscattering effect at the molecule-lead interface due to the use of a small number of gold atoms in the active region of the device. The use of a large number of Au atoms in the active region may reduce the amplitude of the oscillation in $T(E,V)$. Further examination of $T(E,V)$ in Figs. 3(b) and 3(c) reveals an interesting phase-shift behavior between the systems codoped with Na and B and with Li and B; the injection energy for the maximum transmission in the system codoped with Na and B matches that of the minimum transmission in the system codoped with Li and B. The expansion of the cage structure in the system codoped with Na and B compared with that in the system codoped with Li and B, which results in a path difference between the leads, could possibly be the cause for the observed phase change in the transmission.

Since $T(E,V)$ is a unified feature that depends on both the intrinsic properties of the molecule and the electronic structure at the molecule-lead interface, we investigated the role of molecule-lead coupling to identify the origin of the increase in $T(E,V)$ in codoped systems. First, we recalculated the current at 1.99 V for the undoped carborane junction using C_L and C_R extracted at 0.53 V, say I'. We then calculated the ratio between the original current at 1.99 V and I', which is found to be 0.27. A similar approach was adopted to evaluate the ratio for systems codoped with Li and B and with Na and B. For the system codoped with Li and B, we recalculated the current at 1.93 V using the C_L and C_R extracted at 0.53 V; in the system codoped with Na and B the current was recalculated at 1.85 V

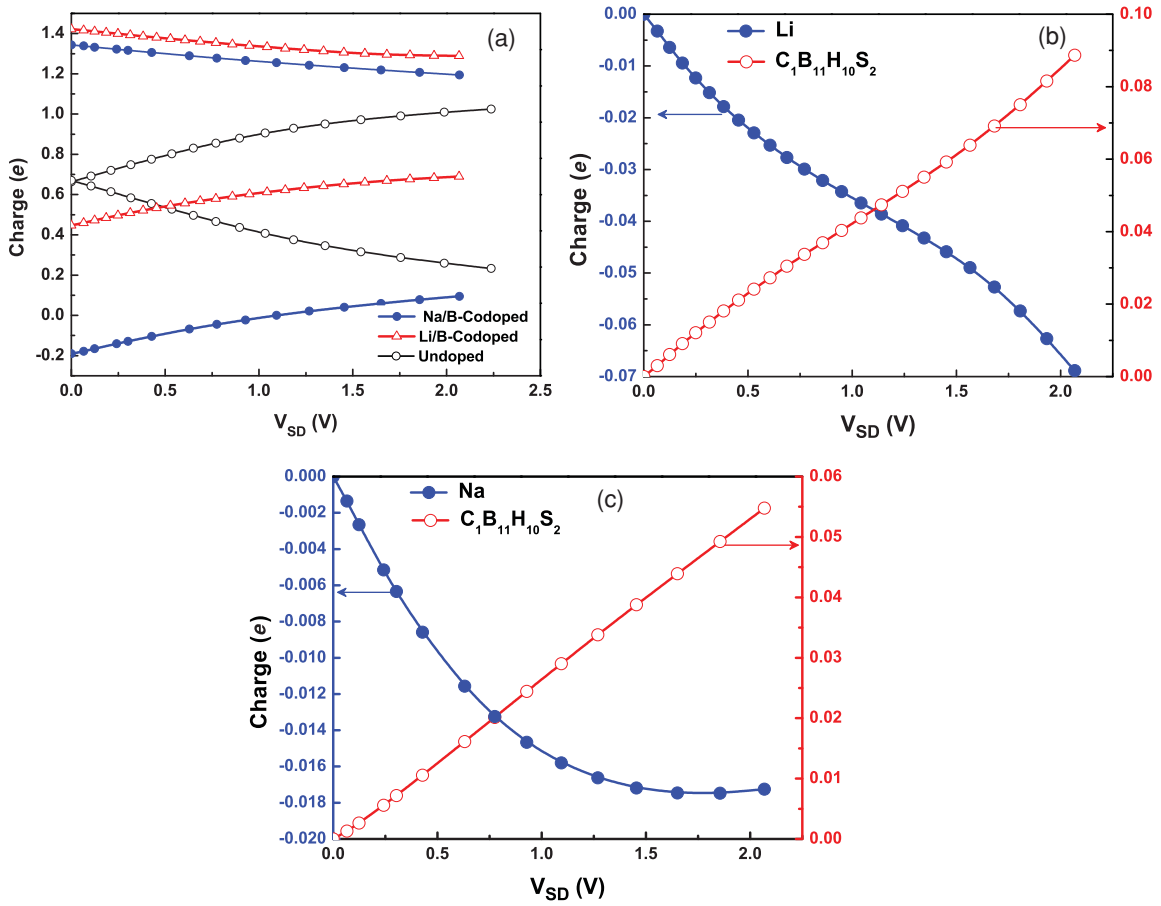

FIG. 4. (Color online) (a) Charge profile characterizing bias-dependent polarization effect on the terminal "S" atoms. (b) Charge profile characterizing bias-dependent polarization effect between the alkali atom and the cage ($C_1B_{11}H_{10}S_2$) in junctions codoped with Li and B, and (c) junctions codoped with Na and B.

using C_L and C_R extracted at 0.43 V. The current ratio for the system codoped with Li and B is found to be 0.73, while for the system codoped with Na and B it is 1.85. This unambiguously suggests that the interfacial coupling changes significantly with increasing bias in the codoped systems, which results in a giant change in conductivity (approximately an order of magnitude in the case of the system codoped with Na and B at ~2 V).

To further understand the increase of $T(E,V)$ for the system codoped with Na and B, we analyzed the density of states at ~ 2 V. The density of states for the system codoped with Na and B is found to be higher than that of the system codoped with Li and B within the chemical-potential window ($\mu_1 = -0.906$ eV, $\mu_2 = 0.949$ eV) as also reflected in the transmission graph in Fig. 3(c). This further confirms the observed increase in current for the system codoped with Na and B.

E. Charge profile

To gain further insight, we analyzed the Mulliken charge on each atom of the device in equilibrium ($V_{\mathrm{HIGH}} = V_{\mathrm{LOW}}$) and nonequilibrium conditions ($V_{\mathrm{HIGH}} \neq V_{\mathrm{LOW}}$). It should be noted that the extended molecule in the active region is always charge-neutral both in the equilibrium and nonequilibrium situations. The bias-dependent charge profiles at the interfacial S atoms for undoped systems and systems codoped with Li and B and with Na and B are summarized in Fig. 4(a). For the undoped system, at equilibrium, both terminal S atoms have the same charge. As the bias increases, the left S atom steadily gains positive charge whereas the right S atom loses positive charge. This bias-induced polarization effect accounts for the valley and the hill at the terminal S atoms in the observed potential profile of the undoped system [Fig. 2(a)]. As expected, due to structural asymmetry at the vertex position in the codoped systems, both terminal S atoms have different charges at equilibrium. The charge asymmetry at the S atoms is much more significant for the system codoped with Na and B. Interestingly, in contrast to the undoped system, the left S atom is found to lose positive charge while the right S atom is found to gain positive charge with increasing V_{SD} in codoped systems. The charge profile of S in codoped systems is also reflected from the observed potential profile described in Figs. 2(c) and 2(d).

To unravel the role of alkali atoms in codoped systems, we also plot the bias-dependent Mulliken charge associated with the alkali atoms as well as the total Mulliken charge associated with $C_1B_{11}H_{10}S_2$ in Figs. 4(b) and 4(c). The charge in the charge axes is scaled by subtracting the respective charge obtained at equilibrium conditions. An intriguing feature is observed by inspecting the charge profile [Figs. 4(b) and 4(c)].

First, we found that the alkali atoms are positively charged, and the negative charge is distributed over $C_1B_{11}H_{10}S_2$ in equilibrium. As bias increases, the alkali atoms gain negative charge while $C_1B_{11}H_{10}S_2$ gains positive charge, suggesting prominent charge transfer from the alkali atoms to $C_1B_{11}H_{10}S_2$ with increasing bias. It is important to mention that a similar charge transfer from dopant atom to host has been observed in a recent experiment, where K atoms were doped into a C_{60} host.[12] For the system codoped with Li and B, the loss of charge from the Li atom is approximately the same as the charge gain by $C_1B_{11}H_{10}S_2$. In contrast, for the system codoped with Na and B, the charge loss from Na is not equal to the charge gain by $C_1B_{11}H_{10}S_2$; charge loss in Na is minimal. Further analysis suggests that there is a strong coupling between the Na atom and the leads via S atoms. In addition, the renormalized density of states for the system codoped with Na and B is found to be higher than that of the system codoped with Li and B within the relevant chemical-potential window. This explains the huge increase in current for the system codoped with Na and B. Since a single alkali atom primarily controls the current-voltage characteristic in the codoped system, we call this device a single-atom-controlled device.

IV. CONCLUSIONS

In summary, we used a codoping model and a parameter-free single-particle Green's function approach in conjunction with the density functional theory to study the role of a dopant atom in a strongly coupled *p*-carborane junction. When compared with the undoped system, at ∼2 V, we found an order-of-magnitude increase in current in the system codoped with Na and B. Compared with the current in the system codoped with Li and B, a twofold increase in current is observed at ∼2 V in the system codoped with Na and B; this suggests that the single alkali atom dictates the electron flow in the codoped junction. Further analysis reveals that alkali atoms donate charge to the $C_1B_{11}H_{10}S_2$ host; the amount of charge transfer varies with the applied bias. This research thus opens the door toward an ultimate limit of miniaturization: where a single atom controls the device characteristics.

ACKNOWLEDGMENTS

We thank Samuel Trickey for helpful discussions during this work and Mathew Durocher for reading this manuscript. This work is supported by NSF through Grant No. 0643420.

[1] P. A. Packan, Science **285**, 2079 (1999).
[2] S. C. Erwin, L. Zu, M. I. Haftel, A. L. Efros, T. A. Kennedy, and D. J. Norris, Nature (London) **436**, 91 (2005).
[3] D. J. Norris, A. L. Efros, and S. C. Erwin, Science **319**, 1176 (2008).
[4] M.-H. Du, S. C. Erwin, and A. L. Efros, Nano Lett. **8**, 2878 (2008).
[5] A. P. Alivisatos, Science **271**, 933 (1996).
[6] O. Seitz, A. Vilan, H. Cohen, C. Chan, J. Hwang, A. Kahn, and C. Cahen, J. Am. Chem. Soc. **129**, 7494 (2007).
[7] X. Zhong, R. Pandey, A. R. Rocha, and S. P. Karna, Phys. Chem. Lett. **1**, 1584 (2010).
[8] M. J. Rosseinsky, A. P. Ramirez, S. H. Glarum, D. W. Murphy, R. C. Haddon, A. F. Hebard, T. T. M. Palstra, A. R. Kortan, S. M. Zahurak, and A. V. Makhija, Phys. Rev. Lett. **66**, 2830 (1991).
[9] A. F. Hebard, M. J. Rosseinsky, R. C. Haddon, D. W. Murphy, S. H. Glarum, T. T. M. Palstra, A. P. Ramirez, and A. R. Kortan, Nature (London) **350**, 600 (1991).
[10] K. Holczer, O. Klein, S.-M. Huang, R. B. Kaner, K.-J. Fu, R. L. Whetten, and F. Diederich, Science **252**, 1154 (1991).
[11] S. P. Kelty, C.-C. Chen, and C. M. Lieber, Nature (London) **352**, 223 (1991).
[12] R. Yamachika, M. Grobis, and W. M. F. Crommie, Science **304**, 281 (2004).
[13] S. R. Schofield, N. J. Curson, M. Y. Simmons, F. J. Rueß, T. Hallam, L. Oberbeck, and R. G. Clark, Phys. Rev. Lett. **91**, 136104 (2003).
[14] P. F. H. Schwab, M. D. Levin, and J. Michl, Chem. Rev. **99**, 1863 (1999).
[15] J. R. Heath and M. A. Ratner, Phys. Today **56**, 43 (2003).
[16] L. I. Zakharkin and A. I. Kovredov, Zh. Obshch. Khim. **44**, 1840 (1974).
[17] L. I. Zakharkin and A. I. Kovredov, Izv. Akad. Nauk SSSR, Ser. Khim. **1428** (1973).
[18] X. G. Yang, W. Jiang, C. B. Knobler, and M. F. Hawthorne, J. Am. Chem. Soc. **114**, 9719 (1992).
[19] J. Muller, K. Base, T. F. Magnera, and J. Michl, J. Am. Chem. Soc. **114**, 9721 (1992).
[20] A. Franken, C. A. Kilner, and J. D. Kennedy, Chem. Commun. **3**, 328 (2004).
[21] R. N. Grimes, J. Chem. Educ. **81**, 658 (2004).
[22] S. Morandi, S. Ristori, D. Berti, L. Panza, A. Beccioloni, and G. Martini, Biochim. Biophys. Acta-Biomembranes. **1664**, 53 (2004).
[23] R. Pati, A. C. Pineda, R. Pandey, and S. P. Karna, Chem. Phys. Lett. **406**, 483 (2005).
[24] W. D. Jemmis and M. M. Balakrishnarajan, J. Am. Chem. Soc. **122**, 7392 (2000).
[25] J. M. Oliva, L. Serrano-Andres, D. J. Klein, P. v. R. Scheleyer, and J. Michl, Int. J. Photoenergy. **2009**, 292393 (2009).
[26] L. Serrano-Andres and J. M. Oliva, Chem. Phys. Lett. **432**, 235 (2006).
[27] W. Zhu, X. Qiu, V. Iancu, X.-Q. Chen, H. Pan, W. Wang, N. M. Dimitrijevic, T. Rajh, H. M. Meyer, M. P. Paranthaman, G. M. Stocks, H. H. Weitering, B. Gu, G. Eres, and Z. Zhang, Phys. Rev. Lett. **103**, 226401 (2009).
[28] R. G. Parr and W. Yang, *Density Functional Theory of Atoms and Molecules* (Oxford, Science, 1994).
[29] GAUSSIAN 03, Gaussian Inc., Pittsburgh, Pennsylvania, USA (2003).
[30] R. Pati, M. McClain, and A. Bandyopadhyay, Phys. Rev. Lett. **100**, 246801 (2008).
[31] J. G. Zhou and F. Hagelberg, Phys. Rev. Lett. **97**, 045505 (2006).
[32] A. Szabo and N. S. Ostlund, *Modern Quantum Chemistry* (Dover, New York, 1996).
[33] F. Evers and K. Burke, *Nano and Molecular Electronics Handbook* (CRC Press, 2007).
[34] P. Delaney and J. C. Greer, Phys. Rev. Lett. **93**, 036805 (2004).
[35] G. Fagas, P. Delaney, and J. C. Greer, Phys. Rev. B **73**, 241314 (2006).

[36]I. Lindgren and J. Morrison, *Atomic Many-Body Theory*, edited by Lambropoulos and H. Walther (Berlin, Springer, 1985).
[37]K. S. Thygesen and A. Rubio, Phys. Rev. B **77**, 115333 (2008).
[38]N. Sai, M. Zwolak, G. Vignale, and M. Di Ventra, Phys. Rev. Lett. **94**, 186810 (2005).
[39]M. Di Ventra, *Electrical Transport in Nanoscale Systems* (Cambridge, New York, 2008).
[40]L. Cheng, J. S. Evans, and T. Van Voorish, Phys. Rev. B **74**, 155112 (2006).
[41]F. Evers, F. Weigend, and M. Koentopp, Phys. Rev. B **69**, 235411 (2004).
[42]E. Runge and E. K. U. Gross, Phys. Rev. Lett. **52**, 997 (1984).
[43]K. Burke, R. Car, and R. Gebauer, Phys. Rev. Lett. **94**, 146803 (2005).
[44]X. Gonze and M. Scheffler, Phys. Rev. Lett. **82**, 4416 (1999).
[45]J. Taylor, H. Guo, and J. Wang, Phys. Rev. B **63**, 245407 (2001).
[46]M. Brandbyge, J. L. Mozos, P. Ordejon, J. Taylor, and K. Stokbro, Phys. Rev. B **65**, 165401 (2002).
[47]Y. Xue, S. Datta, and M. A. Ratner, J. Chem. Phys. **115**, 4292 (2001).
[48]M. Di Ventra, S. T. Pantelides, and N. D. Lang, Phys. Rev. Lett. **84**, 979 (2000).
[49]W. Su, J. Jiang, W. Lu, and Y. Luo, Nano Lett. **6**, 2091 (2006).
[50]G. C. Solomon, C. Herrmann, T. Hansen, V. Mujica, and M. A. Ratner, Nature Chem. **2**, 223 (2010).
[51]A. R. Rocha, V. M. Garcia Suarez, S. W. Bailey, C. J. Lambert, J. Ferrer, and S. Sanvito, Nat. Mater. **4**, 335 (2005).
[52]R. Pati, L. Senapati, P. M. Ajayan, and S. K. Nayak, Phys. Rev. B **68**, 100407 (2003).
[53]P. P. Pal and R. Pati, Phys. Rev. B **82**, 045424 (2010).
[54]A. Nitzan and M. A. Ratner, Science **300**, 1384 (2003).
[55]Vienna *ab initio* Simulation Package, Technische Universität Wien, 1999; G. Kresse and J. Furthmüller, Phys. Rev. B **54**, 11169 (1996).
[56]S. Datta, *Electron Transport in Mesoscopic Systems* (Cambridge University Press, Cambridge, England, 1997).
[57]Y. Meir and N. S. Wingreen, Phys. Rev. Lett. **68**, 2512 (1992).
[58]B. G. Johnson, P. M. W. Gill, J. A. Pople, and D. J. Fox, Chem. Phys. Lett. **206**, 239 (1993).
[59]R. K. Bohn and M. D. Bohn, Inorg. Chem. **10**, 350 (1971).
[60]P. v. R. Schleyer and K. Najafian, Inorg. Chem. **37**, 3454 (1998).
[61]T. P. Fehlner, M. Wu, B. J. Meneghelli, and R. W. Rudolph, Inorg. Chem. **19**, 49 (1980).
[62]G. Vignale and M. Di Ventra, Phys. Rev. B **79**, 014201 (2009).
[63]D. Roy, G. Vignale, and M. Di Ventra, Phys. Rev. B **83**, 075428 (2011).